2011

Adsorption of cobalt ferrite nanoparticles within layer-by-layer films: a kinetic study carried out using quartz crystal microbalance

Physical Chemistry Chemical Physics, Cambridge : Royal Society of Chemistry - RSC, v. 13, n. 48, p. 21233-21242, 2011
http://www.producao.usp.br/handle/BDPI/49346

PCCP

Cite this: *Phys. Chem. Chem. Phys.*, 2011, **13**, 21233–21242

www.rsc.org/pccp

PAPER

Adsorption of cobalt ferrite nanoparticles within layer-by-layer films: a kinetic study carried out using quartz crystal microbalance†

Gustavo B. Alcantara,*[a] Leonardo G. Paterno,[a] André S. Afonso,[b] Ronaldo C. Faria,[b] Marcelo A. Pereira-da-Silva,[c] Paulo C. Morais[a] and Maria A. G. Soler*[a]

Received 22nd August 2011, Accepted 4th October 2011
DOI: 10.1039/c1cp22693b

The paper reports on the successful use of the quartz crystal microbalance technique to assess accurate kinetics and equilibrium parameters regarding the investigation of *in situ* adsorption of nanosized cobalt ferrite particles ($CoFe_2O_4$—10.5 nm-diameter) onto two different surfaces. Firstly, a single layer of nanoparticles was deposited onto the surface provided by the gold-coated quartz resonator functionalized with sodium 3-mercapto propanesulfonate (3-MPS). Secondly, the layer-by-layer (LbL) technique was used to build multilayers in which the $CoFe_2O_4$ nanoparticle-based layer alternates with the sodium sulfonated polystyrene (PSS) layer. The adsorption experiments were conducted by modulating the number of adsorbed $CoFe_2O_4$/PSS bilayers (n) and/or by changing the $CoFe_2O_4$ nanoparticle concentration while suspended as a stable colloidal dispersion. Adsorption of $CoFe_2O_4$ nanoparticles onto the 3-MPS-functionalized surface follows perfectly a first order kinetic process in a wide range (two orders of magnitude) of nanoparticle concentrations. These data were used to assess the equilibrium constant and the adsorption free energy. Alternatively, the Langmuir adsorption constant was obtained while analyzing the isotherm data at the equilibrium. Adsorption of $CoFe_2O_4$ nanoparticles while growing multilayers of $CoFe_2O_4$/PSS was conducted using colloidal suspensions with $CoFe_2O_4$ concentration in the range of 10^{-8} to 10^{-6} (moles of cobalt ferrite per litre) and for different numbers of cycles n = 1, 3, 5, and 10. We found the adsorption of $CoFe_2O_4$ nanoparticles within the $CoFe_2O_4$/PSS bilayers perfectly following a first order kinetic process, with the characteristic rate constant growing with the increase of $CoFe_2O_4$ nanoparticle concentration and decreasing with the rise of the number of LbL cycles (n). Additionally, atomic force microscopy was employed for assessing the LbL film roughness and thickness. We found the film thickness increasing from about 20 to 120 nm while shifting from 3 to 10 $CoFe_2O_4$/PSS bilayers, using the 8.9×10^{-6} (moles of cobalt ferrite per litre) suspension.

Introduction

Adsorption of nanosized materials onto surfaces has been the focus of intensive research activity considering its impact on the investigation of the interaction of nanostructures with biological and non-biological templates, with emphasis ranging from cell labeling to coatings and films.[1–7] Additionally, the increasing growth in the production of nanosized materials nowadays at both laboratory and industrial scales has called special attention to the potential hazardous effects caused by discarding them into the environment, and their binding to organic matter and living organisms.[8] Therefore, investigation regarding the adsorption of nanoparticles onto surfaces, with as diverse composition and function as possible, has become critical to accomplish medical and industrial applications as well as to unveil the path of their dissemination into the environment and their possible damaging effects to living systems.

In this scenario, superparamagnetic iron oxide (SPIO) particles[9] play an important role, since their high magnetization and biocompatibility make them potential nanomaterials for use in biomedicine, as for instance in drug delivery systems,[10] biolabeling,[11] magnetic hyperthermia,[12,13] and magnetic

[a] *Universidade de Brasília, Instituto de Física, Brasília - DF 70910-900, Brazil. E-mail: soler@unb.br, alcantara@fis.unb.br; Fax: +55 6133072363; Tel: +55 6133072900*
[b] *Universidade Federal de São Carlos, Departamento de Química, São Carlos - SP 13565-907, Brazil*
[c] *Instituto de Física de São Carlos, USP, 13560-250, Centro Universitário Central Paulista, UNICEP, 13563-470, São Carlos - SP, Brazil*

† Electronic supplementary information (ESI) available. See DOI: 10.1039/c1cp22693b

resonance imaging contrast enhancers[14,15] among others. Additionally, the use of SPIO particles may also have a profound impact on new industrial technologies as for instance while developing insulating magnetic oil for transformers,[16] structures for spin electronics,[17] bioelectrochemistry,[18] catalysis,[19] and chemical sensing.[20] Specific applications include surface modification of SPIO particles to allow covalent attachment with biomolecules which are then used as molecular recognition sites for sensing. The large surface-to-volume ratio of SPIO particles enhances reaction activity and catalytic efficiency and, hence, improves chemical sensitivity. Indeed, it has been reported that SPIO particles have the capability to increase electron transfer between electrode and molecular recognition sites, such as enzymes.[21]

SPIO particles, as for instance maghemite (γ-Fe_2O_3), magnetite (Fe_3O_4) and cobalt ferrite ($CoFe_2O_4$), display a typical cubic inverse spinel structure and form single domains of about 5–20 nm in diameter. Under wet chemical synthesis approaches SPIO particles can be prepared in large quantities with appreciable control over size, composition, crystallinity, and physical properties (*e.g.* magnetic properties).[22] Furthermore, with proper surface functionalization SPIO particles can be readily dispersed into suitable solvents, thus producing homogeneous and highly stable magnetic fluid (MF) samples.[23,24] Therefore, while using MF samples as a material platform for manipulation and encapsulation of SPIO particles, their adsorption energetics and kinetics on different surfaces, as for instance in metal electrode[25] and polymeric matrix,[26] need to be known in order to provide optimum parameters for their deposition and also to improve loading of recognition sites within the sensor structure.

The quartz crystal microbalance (QCM) technique[27] has already been used to investigate tiny amounts of nanomaterials adsorbed as ultra-thin films.[28–32] The multilayer assembly of nanoparticles (silica or magnetite) and glucose oxidase on charged latex particles was successfully investigated by the QCM technique. It was reported that a single monolayer of either nanoparticle or enzyme was adsorbed at each surface deposition cycle. Additionally, it was found that the introduction of magnetic nanoparticles enhances the effectiveness of the nanoreactor and also combines the benefits of magnetic properties with high surface area.[33] Also, QCM measurements with energy dissipation have been employed to track the adsorption of TiO_2 nanoparticles onto silica in order to evaluate its contamination potential in natural water sub-surface environments. The authors found that water characteristics (*e.g.* pH and ionic strength) play a major role in TiO_2 surface adsorption, in particular adsorption rates are increased when conditions favor electrostatic interactions between nanoparticles and the surface.[34]

Investigations performed on assembling nanoparticles onto the polymeric surface have been focused on the energetic and kinetic features of adsorption.[35] For example, investigation of the adsorption of gold hydrosol (18 nm diameter) onto polystyrene and poly(2-vinylpyridine) films by means of a QCM technique suggested that the particle adsorption is irreversible. At the first stage of adsorption the authors found that the number of adsorbed particles increased linearly with the square root of adsorption time, which characterizes a diffusion-limited adsorption process.[36] Adsorption kinetics and energetic parameters for CdSe–ZnS core–shell quantum dots (3.5 nm diameter) have been attained after treating QCM data using the Langmuir adsorption theory.[37] Irreversible adsorption was identified with adsorption constants being much higher than desorption ones.

In previous investigations we have attained preliminary understanding of the adsorption of citrate-coated maghemite nanoparticles onto doped polyaniline, as well as positively charged bare maghemite onto sodium sulfonated polystyrene (PSS).[38,39] We found that nanoparticles rapidly form a densely-packed layer regardless of the polyelectrolyte type. However, details regarding the adsorbed nanoparticles were limited. Firstly because iron oxide bands in the UV-Vis range are rather structureless, which imparts a significant measurement error. Secondly, no long-term, time-dependent experiment was carried out, including capability for *in situ* absorption observation. In the present contribution, however, we employed the QCM technique to monitor *in situ* and in a long-term regime the adsorption of positively-charged $CoFe_2O_4$ nanoparticles onto bare gold-coated and surface-functionalized QCM resonators and also onto PSS deposited layers. The multilayer deposition was entirely performed inside the QCM cell itself, which allowed continuous monitoring of nanoparticle and polyelectrolyte mass uptake *in situ*. $CoFe_2O_4$ nanoparticles (10.5 nm in diameter) were supplied as ionic colloidal suspension at different nanoparticle concentrations and fixed low-pH value. Data obtained from the QCM measurements allow for robust determination of kinetics (adsorption and desorption constants) and thermodynamics (free energy of adsorption) parameters for adsorption at planar substrates and, additionally, to monitor multilayer film deposition. Further, the adsorption trend was interpreted within the framework of the Langmuir adsorption theory. Moreover, atomic force microscopy (AFM) images of deposited $CoFe_2O_4$/PSS films provided additional information about the $CoFe_2O_4$ nanoparticles adsorption. This investigation was performed in order to improve the understanding of the $CoFe_2O_4$ nanoparticles adsorption onto both a surface-functionalized QCM resonator and onto a polymeric surface, the latter scenario being useful for optimizing nanoparticle loading in functional nanocomposites as well as to serve as a model system to explore the interaction of nanoparticles with polymeric and biological templates.

$CoFe_2O_4$ nanoparticle was chosen as a model system because of its enhanced properties, such as high magnetocrystalline anisotropy, high coercivity, moderate saturation magnetization and high stability at higher temperatures and aggressive chemical media.[40] The presence of surface cobalt atoms also improves catalytic efficiency of $CoFe_2O_4$ nanoparticles towards oxidation of some biochemical substrates, and thus opens up opportunities for applicability as a biosensor. Furthermore, cobalt ferrite nanoparticles have been investigated aiming biomedical applications. Toxicity studies indicated that while using appropriated protocols cobalt ferrite nanoparticles can be reported as biocompatible and could be used as a material platform for biomedical applications.[41–43]

Experimental

Materials

Cobalt nitrate, iron chloride, iron nitrate, sodium sulfonated polystyrene (PSS, M_w 70 000 g mol^{-1}), sodium 3-mercapto propanesulfonate (3-MPS), and 3-mercapto propionic acid (3-MPA) were purchased from Aldrich (USA) and used as received. Perchloric acid, hydrochloric acid, sulfuric acid, sodium hydroxide, and hydrogen peroxide were all analytical grade or better purchased from Merck (Germany) and Synth (Brazil). All water used for nanoparticle synthesis, solution preparations and substrate cleaning was provided by a purification system Milli-Q (water resistivity: 18 MΩ cm^{-1}). PSS solution (1.0 g L^{-1}, pH 1.85) was prepared by dissolving the polyelectrolyte in diluted HCl solution (pH 1.85) under magnetic stirring. Glass slides (BK7, 10 mm × 25 mm × 1 mm) used as substrates for AFM imaging were rendered negatively-charged prior to film deposition by a cleaning procedure, including sequentially a piranha solution (H_2SO_4/H_2O_2, 3 : 1 v/v) followed by RCA solution ($H_2O/H_2O_2/NH_4OH$, 5 : 1 : 1 v/v). QCM experiments were carried out using a 5 MHz AT-cut quartz crystal (QCM 200 STANFORD) with gold electrodes (5 mm in diameter) at both sides.

Synthesis of $CoFe_2O_4$ nanoparticles

Positively-charged $CoFe_2O_4$ nanoparticles were synthesized by co-precipitation of Co(II) and Fe(III) ions in aqueous alkaline medium according to the protocol previously reported[44] and described in short as follows. Concentrated nitric acid (40 mL) was added to previously prepared aqueous solutions of $Co(NO_3)_2$ (0.1 mol L^{-1}, 250 mL) and $FeCl_3$ (0.2 mol L^{-1}, 250 mL) and heated at boiling temperatures (~95 °C) under magnetic stirring. The pH was then raised to 12 with sodium hydroxide solution (3.0 mol L^{-1}), leading to immediate precipitation of $CoFe_2O_4$ nanoparticles. The reaction mixture was cooled down to room temperature and the black precipitate ($CoFe_2O_4$ nanoparticles) was isolated from the supernatant by centrifugation following extensive washing with ultrapure water until neutral pH was reached. The isolated nanoparticles underwent a step of surface passivation by suspending them into $Fe(NO_3)_3$ (0.5 mol L^{-1}) aqueous solution for 30 min, at boiling temperature. The reaction mixture was cooled down to room temperature and the pH was adjusted to 6 with diluted sodium hydroxide (0.1 mol L^{-1}). The precipitate composed of passivated $CoFe_2O_4$ nanoparticles was washed several times with ultrapure water until neutral pH was reached. A stock ionic colloidal suspension was then produced by peptization of nanoparticles using perchloric acid solution (0.25 mol L^{-1}). The acidic medium ensures protonation of nanoparticles' surface sites. Soluble ions, left over in the aqueous phase, were extracted from the fresh MF sample by dialysis against pure water for several days. Hydrodynamic diameter and zeta potential of colloidal suspensions were determined by dynamic light scattering/zeta potential measurements using a Malvern Instrument Zeta Sizer Nano Series ZS90. The hydrodynamic diameter and the ζ-potential for cobalt ferrite nanoparticles suspended within the produced MF sample were found as 41.9 nm and +37.2 mV, respectively. For adsorption studies and film deposition, $CoFe_2O_4$ aqueous dispersions were prepared directly from dilution of the stock ionic MF sample. The concentrations of $CoFe_2O_4$ nanoparticles (expressed in moles of cobalt ferrite per litre) within the used MF samples were set at: S-A 8.9 × 10^{-6} mol L^{-1}; S-B 8.9 × 10^{-7} mol L^{-1}; S-C 3.0 × 10^{-7} mol L^{-1}; S-D 1.3 × 10^{-7} mol L^{-1}; and S-E 8.9 × 10^{-8} mol L^{-1}.

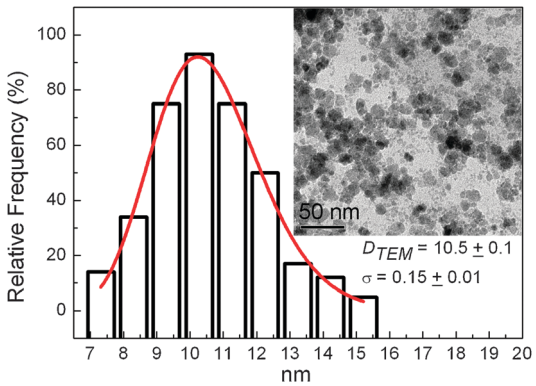

Fig. 1 Particle size histogram of the cobalt ferrite nanoparticles. The inset is a typical TEM micrograph of the sample.

The morphology and size distribution of $CoFe_2O_4$ nanoparticles were assessed by transmission electron microscopy (TEM) employing a JEOL 1011 microscope operating at 100 keV. Fig. 1 presents the particle size histogram (vertical bars) of the $CoFe_2O_4$ sample attained from TEM micrographs (the inset represents a typical TEM micrograph). The parameters describing the nanoparticle size distribution profile were calculated by the standard approach.[45] The solid line in Fig. 1 represents the best curve-fitting using the log-normal distribution function. Values of the average particle diameter (D_{TEM}) and standard diameter deviation (σ) calculated from the curve fitting were 10.5 ± 0.1 nm and 0.15 ± 0.01, respectively. X-Ray diffraction patterns of the powder sample (not shown) referred to cobalt ferrite material in agreement with the JCPDS 22-1086.[46] The chemical composition of nanoparticles, expressed as the [Fe]/[Co] ratio, was determined by atomic absorption spectrometry using a Perkin-Elmer 5000 spectrometer. The ratio [Fe]/[Co] found was 3 : 1.

Quartz crystal microbalance measurements and *in situ* deposition

When homogeneous and rigid ultrathin layers are adsorbed onto the surface of an oscillating crystal the characteristic shift in frequency (Δf) can be related to the increase in mass per unit area (Δm) according to the Sauerbrey equation:[47]

$$\Delta f = -\frac{1}{C_f}\Delta m, \qquad (1)$$

where C_f is the mass sensitivity constant (in our experiments, C_f = 56.6 Hz μg^{-1} cm^2 at 5 MHz). Thus, frequency shifts (Δf) could be converted into mass (Δm) of adsorbed species (nanoparticle and/or polyelectrolyte). The main advantage of this method is the higher sensitivity (nanograms) it provides, which surpasses for instance detection limits imposed by UV-Vis spectroscopy. In the present study, all measurements were conducted at controlled temperature (25 °C) in a

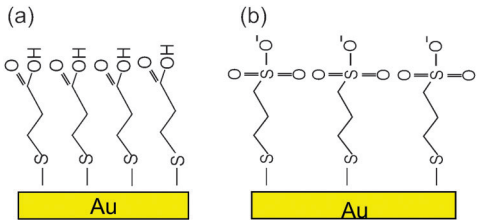

Scheme 1 Chemical structures of (a) 3-mercapto propionic acid (3-MPA) and (b) sodium 3-mercapto propanesulfonate (3-MPS) used to functionalize the gold-plated electrodes.

QCM 200 STANFORD, with the aid of a peristaltic pump (ISMATEC IPC) which allowed the controlled flow of 60 μL min^{-1}. Prior to the experiments, the electrode surface was cleaned using a piranha solution, rinsed with water and left for drying in air. The clean electrodes were further functionalized with sulfonic groups by soaking overnight in an aqueous solution of 3-MPS (0.02 mol L^{-1}). The electrodes were then removed from the 3-MPS solution, rinsed with excess of ultrapure water and left for drying in air. For a control experiment, electrodes were functionalized with carboxylic acid groups using 3-MPA. The chemical structures of 3-MPA and 3-MPS functionalized in the gold electrodes are depicted in Scheme 1.

The as-functionalized electrodes were placed in the QCM cell with one side facing the liquid phase (cleaning solution, nanoparticle dispersion or polyelectrolyte solution) while the other side left exposed to air. At the beginning, the cell was filled with diluted HCl solution (pH 1.85) in order to set the baseline. Afterwards, in order to monitor nanoparticle adsorption on planar functionalized substrates, $CoFe_2O_4$ dispersion was introduced until the cell was completely filled (about 300 μL). The flow was stopped and the adsorption of the first layer of nanoparticles was observed by monitoring the frequency change (Δf) with time (t).

The adsorption of $CoFe_2O_4$ nanoparticles at the PSS polymer surface was also *in situ* monitored. The $CoFe_2O_4$/PSS bilayers were deposited (LbL approach) inside the QCM cell, by simply introducing the nanoparticle dispersion and polyelectrolyte solution alternately, just like it is performed in a current LbL procedure. The mass uptake (Δm) was continuously monitored as a function of time (t). A rinsing step with diluted HCl solution (pH 1.85) was performed after every deposited layer (LbL cycle). Three concentrations of $CoFe_2O_4$ were employed to prepare three different multilayered films, comprising up to ten bilayers, labeled $(CoFe_2O_4/PSS)_{QCM-An}$, $(CoFe_2O_4/PSS)_{QCM-Bn}$ and $(CoFe_2O_4/PSS)_{QCM-En}$, where the subscripts stand for the colloidal suspension concentrations A, B and E, respectively, whereas n represents the number of deposited bilayers.

Deposition of $CoFe_2O_4$/PSS films

In order to study the nanocomposite morphology $CoFe_2O_4$/PSS multilayered films were deposited onto glass slides using the LbL technique. Diluted ionic colloidal dispersions and the PSS polyelectrolyte solution were employed. Cleaned glass slides were firstly immersed into the MF samples (S-A, S-B, or S-E) for 3 min, then rinsed in a stirred HCl solution (pH 1.85) for 30 s and dried under a flow of N_2 gas. In a second step, the substrate containing a layer of positively surface charged nanoparticles was immersed into the anionic solution (PSS) for 3 min, then rinsed and dried as in the nanoparticle layer deposition to produce the first $CoFe_2O_4$/PSS bilayer. Films with up to 10 bilayers were produced by simply repeating the steps described above, originating samples $(CoFe_2O_4/PSS)_{An}$, $(CoFe_2O_4/PSS)_{Bn}$ and $(CoFe_2O_4/PSS)_{En}$ where the subscripts stand for the ionic magnetic colloidal suspensions S-A, S-B or S-E whereas n means the number of bilayers.

The morphological characterization of the as-produced multilayers was assessed by tapping AFM using a Digital MultMode Nanoscope IIIa (silicon tips with a rectangular shaped and cantilever spring constant set at 70 N m^{-1}). Film surface roughness (root-mean-square roughness, R_{rms}) was obtained using the software provided with the instrument. Values measured at three different spots on the sample surface were used to calculate the average R_{rms}. Film thicknesses were also measured by AFM, following a procedure developed by Lobo *et al.*[48]

Results and discussion

$CoFe_2O_4$ nanoparticle adsorption onto QCM crystals modified with 3-MPS

Fig. 2a displays the time-dependence of Δf during adsorption of $CoFe_2O_4$ nanoparticles onto QCM crystals surface-modified with 3-MPS. The adsorption process was investigated in the time window of 1150 seconds at different $CoFe_2O_4$ nanoparticle concentrations (MF samples S−A, S−B, and S−E)

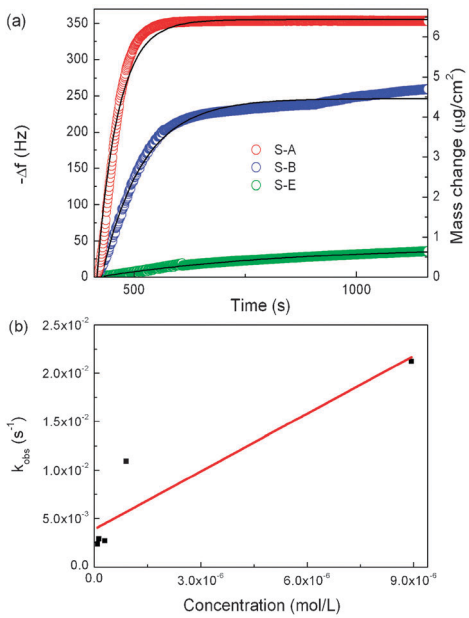

Fig. 2 (a) Time dependence of frequency shift for nanoparticle adsorption onto QCM crystals modified with 3-MPS, at different $CoFe_2O_4$ nanoparticle concentrations and fixed pH (1.85). The mass change (right hand-side scale) was calculated from eqn (1). The experimental data (colored symbols) were fitted (solid black lines) with a first order chemical process, as described by eqn (2). (b) k_{obs} values obtained (solid squares) were plotted as a function of nanoparticle concentration. The data were fitted (solid red line) with a linear equation (eqn (3)).

Table 1 k_{obs} and $\Gamma(\infty)$ values attained after fitting the experimental data (see Fig. 2a) of cobalt ferrite nanoparticles adsorbed onto a 3-MPS modified gold surface as a function of nanoparticle concentration and pH 1.85

MF sample	k_{obs}/s^{-1}	$\Gamma(\infty)$/Hz
S-A	$(2123 \pm 40) \times 10^{-5}$	355.0 ± 0.4
S-B	$(1091 \pm 10) \times 10^{-5}$	246.0 ± 0.4
S-C	$(267 \pm 1) \times 10^{-5}$	204.0 ± 0.6
S-D	$(287 \pm 2) \times 10^{-5}$	81.0 ± 0.2
S-E	$(234 \pm 3) \times 10^{-5}$	43.0 ± 0.2

and fixed pH (1.85), as indicated. In the investigated time window the saturation of the QCM frequency shift was reached for all nanoparticle concentrations employed. Note that saturation for samples with higher nanoparticle concentration (MF samples S−A and S−B) is reached faster, around 660 seconds, whereas for the lower nanoparticle concentration employed (MF sample S−E) saturation was reached at longer times, around 1000 seconds. In addition, it was observed that the more concentrated the colloidal suspension is the greater the amount of adsorbed nanoparticles, reaching 6.4 μg cm^{-2} while using MF sample S−A. The asymptotic behavior of the adsorbed mass of nanoparticles as a function of time suggests the occurrence of a first order kinetics process. To support this hypothesis we fitted the experimental data with a first order adsorption process equation described by

$$\Gamma(t) = \Gamma(\infty)[1 - \exp(-k_{obs}t)], \quad (2)$$

where $\Gamma(t)$ is the adsorbed amount in μg cm^{-2} at time t, $\Gamma(\infty)$ is the adsorbed amount at infinite time and k_{obs} is the characteristic rate constant. The $\Gamma(\infty)$ and k_{obs} values obtained from our fitting (see Fig. 2a) are collected in Table 1. Fig. 2a shows a very good agreement between the experimental data (colored symbols) and the fitting (solid black lines), thus supporting our hypothesis of a first order kinetics process for nanoparticle's adsorption. Adsorption of CdSe/Zn quantum dots[37] and gold nanoparticles[49] onto planar substrates also follows a first order kinetic process.

The observed rate constant k_{obs} included in eqn (2) can be expressed as:[50]

$$k_{obs} = k_a C + k_d, \quad (3)$$

where C is the nanoparticle concentration in the colloidal suspension (in moles of $CoFe_2O_4$ per litre) and k_a and k_d are adsorption and desorption constants, respectively. The linear relationship observed between k_{obs} and C was fitted by the red solid line shown in Fig. 2b. From that fitting it was possible to estimate adsorption and desorption constants, as collected in Table 2.

Table 2 Adsorption parameters k_a and k_d attained from the linear fitting shown in Fig. 2b and related to cobalt ferrite nanoparticles adsorbed onto a 3-MPS modified gold surface, at pH 1.85. The calculated equilibrium constant and the free energy are represented by K and ΔG^{o}_{ads}, respectively

$k_a/(mol/L)^{-1}\ s^{-1}$	k_d/s^{-1}	$K/(mol/L)^{-1}$	ΔG^{o}_{ads}/ kcal mol^{-1}
$(2.0 \pm 0.4) \times 10^3$	$(4 \pm 1) \times 10^{-3}$	$(0.5 \pm 0.1) \times 10^6$	-7.8 ± 0.1

The adsorption of $CoFe_2O_4$ nanoparticles onto planar substrates occurs at a significantly higher rate than desorption, as we found k_a to be greater than k_d (see values collected in Table 2). The equilibrium constant for the process, as calculated from $K = k_a/k_d$, is equal to 0.5×10^6 $(mol/L)^{-1}$, which is within the range of values reported in the literature for CdSe/ZnS core–shell nanoparticles (3.5 nm) or Au nanoparticles (~10 nm) assembled onto the amine-terminated surface.[37,49] This finding evidences a strong association between $CoFe_2O_4$ nanoparticles and the substrate surface. Considering a model picture for the system in which all surface sites are occupied, with adsorbed nanoparticles forming a monolayer composed of a hexagonal close-packed arrangement of spheres, a simple calculation gives 2.0×10^{12} nanoparticles per cm^2. Note that narrow particle size distribution, as we found in the colloidal dispersion employed ($\sigma = 0.15 \pm 0.01$), is a key point for spontaneous dimer formation in $CoFe_2O_4$ aqueous dispersions.[51] Additionally, dimers are favorable units for organizing hexagonal close-packed arrangement of spheres on a hosting surface. Based on this model picture, the nanoparticle surface coverage of planar substrates could be estimated at 92%, 64%, 53%, 21% and 11% while using the MF samples S-A, S-B, S-C, S-D and S-E, respectively. The total coverage is a limiting case, even while using concentrated MF samples (S-A for instance), as all available sites at the hosting surface are fully occupied and less favorable adsorption sites may also appear at the surface. Moreover, some nanoparticle clustering is expected to occur at higher particle concentration as confirmed by the AFM analysis performed in this study (see below). The total surface coverage reported here far outweighs those reported for the adsorption of γ-Fe_2O_3 nanoparticles onto mica and gold flat substrates, which reached a maximum of 20%.[25] As already pointed out by Semmler *et al.*,[52] smaller particles are capable of adsorbing within the voids inaccessible to the large ones and, consequently, the maximal surface coverage is increased with respect to the monodisperse case. In addition, the investigations regarding adsorption of magnetic nanoparticles rarely consider the inherent dipolar interactions, which are strong enough to overcome electrostatic repulsions and thus enhance the surface coverage. Since the adsorption kinetics of $CoFe_2O_4$ is of first order, the rate (and the amount adsorbed) increases as the adsorbate (nanoparticle) concentration increases. Thus, if the nanoparticle concentration in the deposition fluid is low, the amount of adsorbed nanoparticles is low as well. In more concentrated fluids, some nanoparticle aggregation is possible, but the estimative of substrate covering suggests for compact layers rather than aggregation. The partial surface coverage, however, is attributed to both the reduced number of nanoparticles available in more diluted magnetic colloidal dispersions (like S-D and S-E) and the repulsive interaction among the already adsorbed nanoparticle and the incoming ones.

Once K is known the standard free energy of the nanoparticle adsorption can be estimated from the fundamental equation of equilibrium, $\Delta G^{o}_{ads} = -RT\ln K$. As quoted in Table 2 ΔG^{o}_{ads} is negative, as expected for a spontaneous process. In most cases, where the electrostatic attraction occurs between oppositely charged species, adsorption is a spontaneous process.[37,53,54] The decrease in the free energy as the adsorption proceeds is favored by entropy variation, which

increases due to the release of water molecules and counterions by the hosting substrate and adsorbed nanoparticles, thus increasing the degree of disorder in the surroundings (*e.g.* the nanoparticle dispersion).

The equilibrium state of the adsorption process of $CoFe_2O_4$ nanoparticles onto planar substrates was additionally investigated taking into account the Langmuir adsorption theory, which relates the fractional coverage of the surface with the concentration (C) of the adsorbed species, at a particular temperature (isotherm). In the simplest case it is assumed that every adsorption site is equivalent and the probability of a particle to bind at the site is not influenced by occupied neighboring sites. The Langmuir isotherm equation is given by:

$$\Gamma = \frac{\Gamma_{max} K_L C}{1 + K_L C}, \quad (4)$$

where Γ is the adsorbed amount in μg cm^{-2} and Γ_{max} is the maximum amount of adsorbed nanoparticles (or maximum surface coverage). Rearranging the Langmuir equation (eqn (4)) one obtains its linear form:

$$\frac{C}{\Gamma} = \frac{1}{\Gamma_{max} K_L} + \frac{C}{\Gamma_{max}}. \quad (5)$$

As the QCM frequency shift (Δf) scales with the adsorbed mass (Δm) Fig. 3a shows the nanoparticle concentration dependence of the equilibrium QCM frequency shift (after 20 min adsorption isotherm), as obtained from the data plotted in Fig. 2a. The red solid line in Fig. 3a represents the best curve fitting using eqn (4). From the curve fitting procedure shown in Fig. 3a we found $\Gamma_{max} = 6.51$ μg cm^{-2}. This value is equivalent to the calculated mass of a two-dimensional close-packed arrangement of 2.0×10^{12} spherical $CoFe_2O_4$ particles, as described above. The linear form of the Langmuir equation was used to fit (solid line) the experimental data (symbols) of C/Γ *versus* C, as shown in Fig. 3b. Note, from Fig. 3b, the good agreement between the experimental data (symbols) and the linear form of the Langmuir equation (red solid line).

The equilibrium constant K_L value estimated from the Langmuir isotherm shown in Fig. 3 is 2.1×10^6 (mol/L)$^{-1}$, whereas the value found from the kinetic study is 0.5×10^6 (mol/L)$^{-1}$. Despite the experimental error, the order of magnitude of both values is comparable and indicates a strong interaction between $CoFe_2O_4$ nanoparticles and the sulfonic groups used to functionalize the substrate surface. In a previous experiment we have conducted the adsorption of $CoFe_2O_4$ nanoparticles onto crystals surface-modified with 3-MPA, in which case we observed a less-pronounced surface adsorption. We have attributed the less-pronounced adsorption to the reduced number of negatively-charged adsorption sites at the crystal surface, once under pH 1.85 the 3-MPA molecule remains protonated (–COOH pK_a around 4.7). On the other hand, surface-functionalization of microbalance crystals with 3-MPS provided sulfonic groups which remain negatively charged over a broader pH range (–SO_3 pK_a is about 0.7) and thus available (negatively charged) for nanoparticle adsorption. According to these findings it can be concluded that the adsorption of positively-charged $CoFe_2O_4$ nanoparticles is mainly driven by electrostatic attraction due to negatively-charged sites at the gold-plated and functionalized substrate surface.

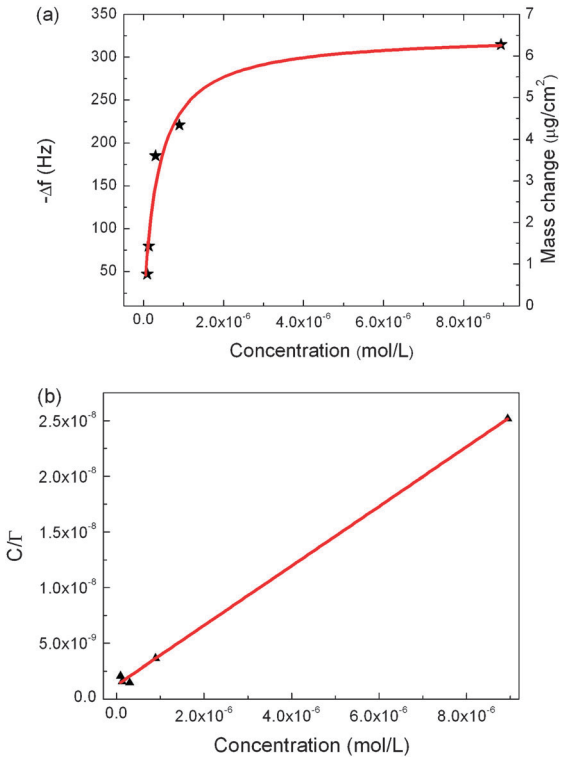

Fig. 3 (a) Langmuir adsorption isotherm of cobalt ferrite nanoparticles adsorbed onto a 3-MPS modified gold surface, at pH 1.85. Symbols represent the data plotted in Fig. 2a whereas the red solid line is the best fitting using eqn (4). (b) Linear form of the Langmuir plot for cobalt ferrite nanoparticles adsorbed onto a 3-MPS modified gold surface. Symbols represent the data plotted in Fig. 2a whereas the red solid line is the best fitting using eqn (5).

Multilayer deposition onto planar substrates

The adsorption kinetics of $CoFe_2O_4$ nanoparticles within the multilayered LbL film was also investigated *in situ* by employing magnetic fluid samples at different nanoparticle concentrations (pH 1.85) and fixed polyelectrolyte concentration. Fig. 4 shows the entire adsorption cycles of $CoFe_2O_4$/PSS multilayered LbL films while monitored by QCM, with the inset in Fig. 4a indicating each separate adsorption step. This periodic behavior is ensured by the reversal of the net surface charge after complete adsorption of each layer. Note that the periodic adsorption behavior was observed for a time window larger than eleven hours while assembling $(CoFe_2O_4/PSS)_{QCM-A10}$ (Fig. 4a) and $(CoFe_2O_4/PSS)_{QCM-B10}$ films (Fig. S1, ESI†). However, the more diluted suspension (S-E) imposed a less regular film growth (see Fig. 4b), which is interrupted after absorption of a few bilayers. Since the adsorption is driven by electrostatic interactions it is reasonable to conclude that the reduced concentration of $CoFe_2O_4$ nanoparticles in sample S-E responds to a continuous decrease in the number of positive surface sites, which thus gradually reduces the adsorption until it stops completely.

Representative pictures of the multilayer deposition ($CoFe_2O_4$/PSS nanofilms) are shown in Fig. 5, which displays adsorption isotherms for the 1st, 3rd, 5th and 10th $CoFe_2O_4$ nanoparticle layers using the magnetic colloidal suspensions S-A.

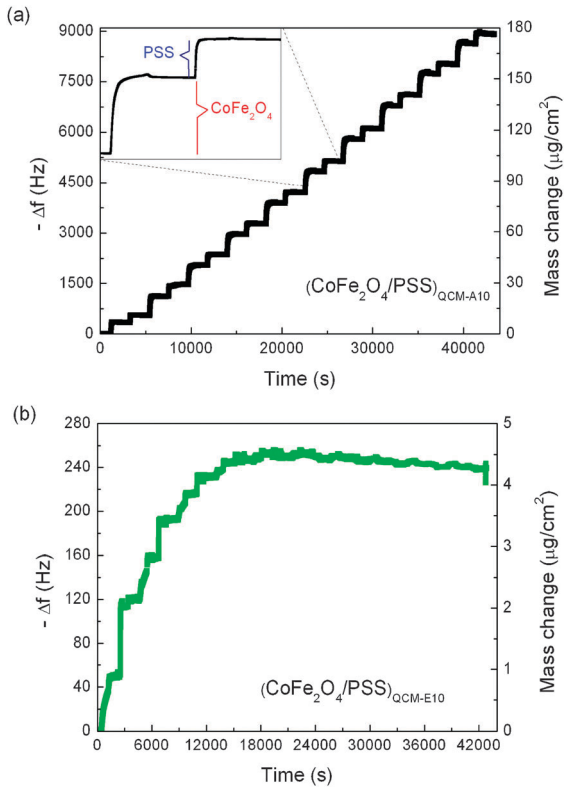

Fig. 4 Deposition of multilayered films of (a) $(CoFe_2O_4/PSS)_{QCM-A10}$ and (b) $(CoFe_2O_4/PSS)_{QCM-E10}$ monitored by QCM for a time window larger than eleven hours. Magnetic dispersions (at different nanoparticle concentrations) and fixed polyelectrolyte concentration were introduced alternately into the QCM cell (*in situ*), which mimics a LbL procedure. The inset in Fig. 4a indicates individual adsorption steps.

It can be clearly seen that the Δf saturation values take longer to be reached the farther the $CoFe_2O_4$/PSS layers are from the substrate surface. While using sample S-A to grow the nanofilm we found that the amount of the $CoFe_2O_4$ nanoparticles at the very first layer is smaller (6.4 μg cm^{-2}—1st) than the amount found at latter layers: 10.5 μg cm^{-2}—3rd; 11.2 μg cm^{-2}—5th; and 11.8 μg cm^{-2}—10th. The same trend was observed while using the sample S-B (Fig. S2, ESI†), with

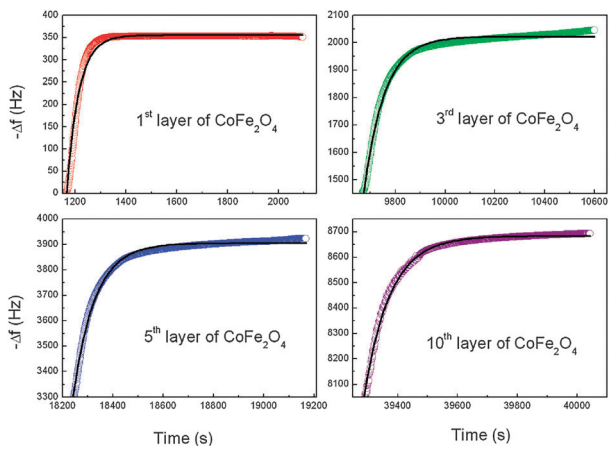

Fig. 5 Adsorption isotherms for the 1st, 3rd, 5th, and 10th $CoFe_2O_4$ nanoparticle layers, assembled using colloidal dispersion samples S-A.

Table 3 k_{obs} values obtained from cobalt ferrite nanoparticles (from MF samples S-A and S-B) adsorbed onto a 3-MPS modified gold surface at pH 1.85. The data were obtained by using eqn (2) to perform the fitting of the experimental data

Sample (S-A)	k_{obs}/s^{-1}	Sample (S-B)	k_{obs}/s^{-1}
1st layer	$(2123 \pm 40) \times 10^{-5}$	1st layer	$(1091 \pm 100) \times 10^{-5}$
3rd layer	$(1214 \pm 8) \times 10^{-5}$	3rd layer	$(550 \pm 5) \times 10^{-5}$
5th layer	$(1161 \pm 7) \times 10^{-5}$	5th layer	$(508 \pm 4) \times 10^{-5}$
10th layer	$(1155 \pm 6) \times 10^{-5}$	10th layer	$(435 \pm 2) \times 10^{-5}$

4.4 μg cm^{-2} for the first layer; 6.3 μg cm^{-2}—3rd; 6.4 μg cm^{-2}—5th; and 6.5 μg cm^{-2}—10th. The key difference between adsorption of a single layer of nanoparticles onto the substrate surface and a multilayer scenario is clear; the net amount of nanoparticles is greater at the top of already deposited bilayers, just because the number of charged sites and the available surface area is greater at the bilayers than it is at the bottom (plain substrate).

Table 3 collects the values of k_{obs} obtained by fitting the experimental data shown in Fig. 5 while using the first order kinetics process described by eqn (2), at different bilayer numbers (n). We found that the fitted k_{obs} values decrease monotonically as the number (n) of deposited bilayers increases or, alternatively, as the distance from the bottom (close to the substrate surface) to the top increases. Our observation is rationalized as follows. Once adsorbed onto the very first flat surface nanoparticles have little chance to move around for better accommodation or re-organization and that explains the fast initial deposition process. Note that the adsorption of the first nanoparticle layer takes place at the QCM crystal (*in situ*), which provides a very flat and immobile surface. Within the multilayer deposition scenario, however, subsequent adsorption occurs at a rougher surface formed by previous deposited layers of $CoFe_2O_4$ nanoparticles embedded into PSS. PSS chains present a significant mobility when they get hydrated during depositions and thus they hinder the diffusion of nanoparticles which imparts longer times of adsorption. However, the longer adsorption time within the multilayers is also attributed to a greater number of negatively-charged sites provided by PSS chains. Since more nanoparticles have to be adsorbed, a longer time is necessary for all these particles to reach equilibrium positions. Therefore, at higher numbers (n) of deposited bilayers the nanoparticle adsorption becomes slower as it takes longer for the nanoparticle to find out equilibrium sites and because a greater number of nanoparticles have to be adsorbed to compensate the negatively-charged sites provided by PSS chains. Actually, we observed from AFM measurements that surface roughness tends to increase as the number (n) of deposited bilayers increases.

Adsorption of $(CoFe_2O_4/PSS)$ films onto glass slides

Fig. 6 shows AFM images (topography and amplitude) of the LbL $(CoFe_2O_4/PSS)_{Bn}$ films with n = 1, 3, 5 and 10 bilayers deposited onto glass slides. Regardless of the layer number (n), the typical globular morphology involving $CoFe_2O_4$ nanoparticles predominates, which spread throughout the entire surface forming a densely-packed layer. Clustering has been also observed, especially in films with several bilayers, as in

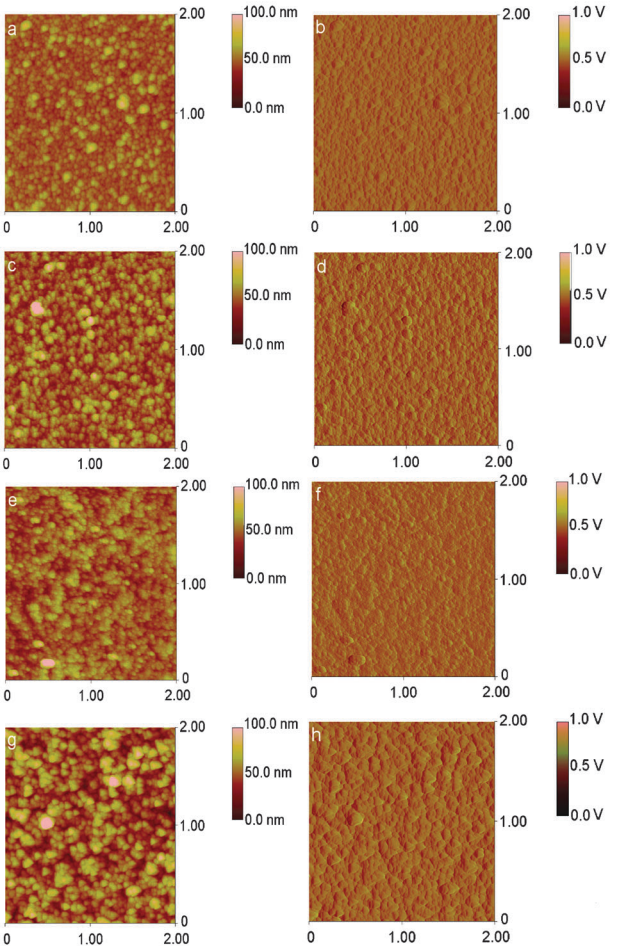

Fig. 6 Typical tapping-mode AFM images ($1 \times 1\ \mu m^2$) of $(CoFe_2O_4/PSS)_{Bn}$ films, showing the topography (left panels) and the amplitude (right panels). The number of bilayers (n) are $n = 1$ (a, b), $n = 3$ (c, d), $n = 5$ (e, f), and $n = 10$ (g, h).

Fig. 6e and g. Surface roughness values of $CoFe_2O_4$/PSS films, with different n numbers and fabricated using different magnetic fluid samples (S-A, S-B, and S-E) are collected in Table 4. Note from the data included in Table 4 that surface roughness increases as the number (n) of $CoFe_2O_4$/PSS bilayers increases, especially while using samples S-A and S-B with higher nanoparticle concentration. Films deposited using the MF sample S-E reveal only small changes in the surface roughness.

The roughness increase reported in this study is expected for this type of bottom-up construction simply because defects are naturally formed at the freshly formed surface and act as nuclei for film growth. For instance, agglomeration is usually driven by reduction of the high surface energy when nanoparticles adsorb onto themselves. Additionally, the polyelectrolyte also plays its role by coating individual and clustered nanoparticles and thus increasing the layer surface area. The top surface becomes more irregular or even fractal as more layers are being adsorbed and this new condition favors the adsorption of even more material, as we have observed in the QCM measurements. This effect is usually observed in LbL films made of polyelectrolytes only and has also been reported for films fabricated while alternating polyelectrolytes with nanoparticles of different chemical compositions, including iron oxides, Au, TiO_2, carbon, and graphene platelets.[36,38,55] Note that the nearly constant surface roughness observed for the film fabricated using the most diluted (8.9×10^{-8} mol L^{-1}) MF sample S-E (data in the last line of Table 4) we attribute to the low surface coverage at the very first layer (11%) and on the subsequent layers ($n = 3$, 5, 10), which limits the surface adsorption to very low amounts.

Table 4 Surface roughness values (in units of nm) taken from AFM data of $(CoFe_2O_4/PSS)_{An}$, $(CoFe_2O_4/PSS)_{Bn}$, and $(CoFe_2O_4/PSS)_{En}$ films deposited onto glass slides, using magnetic colloidal suspensions S-A, S-B, and S-E

Films	$n = 1$	$n = 3$	$n = 5$	$n = 10$
$(CoFe_2O_4/PSS)_{An}$	2.1	5.6	8.3	10.7
$(CoFe_2O_4/PSS)_{Bn}$	6.9	9.2	11.0	14.7
$(CoFe_2O_4/PSS)_{En}$	2.1	2.1	3.3	3.5

The AFM data show amplitude images (Fig. 6, right hand-side panels) in which the contour of nanoparticles is clearly seen though no contrast difference is observed among films with different numbers (n) of $CoFe_2O_4$/PSS bilayers. As typical of LbL films the deposited surface is composed of both cationic/anionic materials distributed homogeneously onto the surface. Moreover, the topmost layer in all samples is made of PSS, which ensures identical chemical composition and tribologic properties. However, one should expect differences when topmost layers of different compositions are compared. We have observed changes in the amplitude images of $CoFe_2O_4$/PEDOT:PSS LbL films when comparing samples with the topmost layer made of $CoFe_2O_4$ nanoparticles or PEDOT:PSS.[56] Despite the homogenous distribution of each material when the topmost layer was composed of $CoFe_2O_4$ nanoparticles the contour of nanoparticles was clearly seen. On the other hand, when the topmost layer comprises PEDOT:PSS the contours were less evident because the polymeric material fills in the voids left over around nanoparticles. Damping forces experimented by the AFM tip were substantially different to generate distinct images for each terminated surface.

Estimation of the nanofilm thickness was independently performed by AFM evaluation. The AFM tip was used to scratch and peel out a small spot of the film deposited onto the

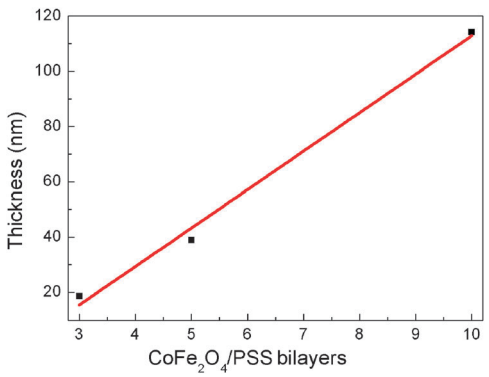

Fig. 7 Dependence of the film thickness using AFM on the number of $CoFe_2O_4$/PSS bilayers, assembled with colloidal dispersion sample S-A. Deposition conditions: pH 1.85; [PSS] = 1.0 g L^{-1} at pH 1.85.

solid substrate in order to create a step (see, for instance, Fig. S3a and b, ESI†), allowing estimation of the film thickness. A linear dependence was found between the film thickness and the number of nominal $CoFe_2O_4$/PSS bilayers (see Fig. 7), indicating that the cycling assembly provides an increasing adsorption of cobalt ferrite nanoparticles and PSS with fine control of the film thickness and structure. After 10 cycles the film thickness as attained from the AFM evaluation shown in Fig. 7 is 114 nm.

Conclusions

In this paper the quartz crystal microbalance (QCM) technique was successfully employed to assess kinetic and equilibrium parameters related to the adsorption of nanosized cobalt ferrite particles (10.5 nm-diameter) onto two different surfaces, namely a single layer of cobalt ferrite ($CoFe_2O_4$) nanoparticles onto the surface of a gold-coated quartz resonator functionalized with sodium 3-mercapto propanesulfonate (3-MPS) and within a multilayer structure consisting of alternated layers of $CoFe_2O_4$ nanoparticles and sodium sulfonated polystyrene (PSS), the multilayer structure being grown by the layer-by-layer (LbL) approach. All experiments were conducted *in situ* within the QCM and allowed the determination of the Langmuir constant (K_L) and the adsorption free energy (ΔG^{o}_{ads}). The formation of densely-packed layers of $CoFe_2O_4$ nanoparticles onto the surface-functionalized electrodes takes no longer than 11 minutes, with magnetic colloidal dispersions containing at least 10^{-4} g of cobalt ferrite per litre. Using more diluted MF samples the surface coverage is incomplete and the saturation plateau cannot be reached at the time window of our investigation (up to 20 minutes). The huge kinetics adsorption and equilibrium constants found for the process indicate a strong electrostatic interaction between the nanoparticle's positively-charged surface and the negative sulfonic groups at the functionalized QCM electrode. Under equilibrium conditions, the adsorption of $CoFe_2O_4$ nanoparticles can be described by the Langmuir adsorption theory. The maximum surface coverage determined by the Langmuir isotherm agrees quite well with the adsorbed mass predicted by the model picture proposed for a compact layer of nanoparticles, with spherical particles composing a two-dimensional hexagonal close-packed array. The free-energy of adsorption of $CoFe_2O_4$ nanoparticles is negative, as expected for a spontaneous process. Likewise, the absorption of $CoFe_2O_4$ nanoparticles within multilayers of $CoFe_2O_4$/PSS follows a first order kinetic process. However, the adsorption of nanoparticles takes longer at the top of already deposited $CoFe_2O_4$/PSS bilayers than it does at the plain QCM electrode. This finding we hypothesize is related to the increasing surface roughness at the top bilayers, leading to the decrease of the nanoparticle surface diffusivity and thus increasing the time the nanoparticle spends to find out equilibrium sites. Atomic force microscopy (AFM) pictures and morphology data confirm our hypothesis. However, the mass of nanoparticles is virtually the same on each bilayer, which thus leads to the conclusion that despite kinetics the amount of adsorbed species is mainly regulated by the electrostatic attraction and charge compensation inside the multilayer structure. Indeed, our findings show that the combination of *in situ* QCM measurements and models of adsorption can provide fundamental information regarding the adsorption of nanoparticles onto planar surfaces. This information is extremely important as far as different aspects of nanoparticle science and technology are concerned, in particular to address issues related to nanoecotoxicology and remediation, biological risks, and biomedical applications.

Acknowledgements

The financial support from the Brazilian agencies MCT/CNPq, FINEP, CAPES, FUNAPE, and FINATEC is gratefully acknowledged. The authors acknowledge Dr Emilia C.D. Lima (Universidade Federal de Goiás, Brazil) for supplying the magnetic fluid samples, Dr Fernando J. Fonseca (Universidade de São Paulo, Brazil) for sample preparation facilities, and Dr Sonia Nair Bao (Universidade de Brasília, Brazil) for TEM facilities.

Notes and references

1 J. Zhou, G. Romero, E. Rojas, L. Ma, S. Moya and C. Gao, *J. Colloid Interface Sci.*, 2010, **345**, 241.
2 D. A. Gorin, S. A. Portnov, O. A. Inozemtseva, Z. Luklinska, A. M. Yashchenok, A. M. Pavlov, A. G. Skirtach, H. Möhwald and G. B. Yashchenok, *Phys. Chem. Chem. Phys.*, 2008, **10**, 6899.
3 M. H. Yang, F. L. Qu, Y. S. Lu, G. L. Shen and R. Q. Yu, *Talanta*, 2008, **74**, 831.
4 S. Dey, K. Mohanta and A. J. Pal, *Langmuir*, 2010, **26**, 9627.
5 M. A. G. Soler, S. N. Bao, G. B. Alcantara, V. H. S. Tiburcio, G. R. Paludo, J. F. B. Santana, M. H. Guedes, E. C. D. Lima, Z. G. M. Lacava and P. C. Morais, *J. Nanosci. Nanotechnol.*, 2007, **7**, 1069.
6 E. Amstad, S. Zurchr, A. Mashaghi, J. Y. Wong, M. Textor and E. Reimhult, *Small*, 2009, **5**, 1334.
7 X. Su, B. S. Kim, S. R. Kim, P. T. Hammond and D. J. Irvine, *ACS Nano*, 2009, **3**, 3719.
8 A. K. Madl and K. E. Pinkerton, *Crit. Rev. Toxicol.*, 2009, **39**, 629.
9 S. Bedanta and W. Kleemann, *J. Phys. D: Appl. Phys.*, 2009, **42**, 013001.
10 T. Islam and L. Josephson, *Cancer Biomarkers*, 2009, **5**, 99.
11 S. Mazzucchelli, M. Colombo, C. De Palma, A. Salvadè, P. Verderio, M. D. Coghi, E. Clementi, P. Tortora, F. Corsi and D. Prosperi, *ACS Nano*, 2010, **4**, 5693.
12 R. S. Rachakatla, S. Balivada, G. M. Seo, C. B. Myers, H. Wang, T. N. Samarakoon, R. Dani, M. Pyle, F. O. Kroh, B. Walker, X. Leaym, O. B. Koper, V. Chikan, S. H. Bossmann, M. Tamura and D. L. Troyer, *ACS Nano*, 2010, **4**, 7093.
13 C. Minelli, S. B. Lowe and M. M. Stevens, *Small*, 2010, **6**, 2336.
14 M. F. Casula, P. Floris, C. Innocenti, A. Lascialfari, M. Marinone, M. Corti, R. A. Sperling, W. J. Parak and C. Sangregorio, *Chem. Mater.*, 2010, **22**, 1739.
15 M. Mahmoudi, M. A. Sahraian, M. A. Shokrgozar and S. Laurent, *ACS Chem. Neurosci.*, 2011, **2**, 118.
16 W. R. Viali, G. B. Alcantara, P. P. C. Sartoratto, M. A. G. Soler, E. Mosinievicz-Szablewska, B. Andrzejewski and P. C. Morais, *J. Phys. Chem. C*, 2010, **114**, 179.
17 P. N. Hai, S. Ohya and M. Tanaka, *Nat. Nanotechnol.*, 2010, **5**, 593.
18 J. D. Qiu, H. P. Peng, R. P. Liang and X. H. Xia, *Biosens. Bioelectron.*, 2010, **25**, 1447.
19 C. W. Lim and I. S. Lee, *Nano Today*, 2010, **5**, 412.
20 L. Stanciu, Y. H. Won, M. Ganesana and S. Andreescu, *Sensors*, 2009, **9**, 2976.
21 I. Willner, R. Baron and B. Willner, *Biosens. Bioelectron.*, 2007, **22**, 1841.
22 M. A. Willard, L. K. Kurihara, E. E. Carpenter, S. Calvin and V. G. Harris, *Int. Mater. Rev.*, 2004, **49**, 125.
23 M. A. G. Soler, G. B. Alcantara, F. Q. Soares, W. R. Viali, P. P. C. Sartoratto, J. R. L. Fernandez, S. W. da Silva, V. K. Garg, A. C. Oliveira and P. C. Morais, *Surf. Sci.*, 2007, **601**, 3921.

24 M. A. G. Soler, E. C. D. Lima, E. S. Nunes, F. L. R. Silva, A. C. Oliveira, R. B. Azevedo and P. C. Morais, *J. Phys. Chem. A*, 2011, **115**, 1003.
25 I. T. Lucas, E. Dubois, J. Chevalet and S. Durand-Vidal, *Phys. Chem. Chem. Phys.*, 2008, **10**, 3263–3273.
26 Y. Wang, L. Hosta-Rigau, H. Lomas and F. Caruso, *Phys. Chem. Chem. Phys.*, 2011, **13**, 4782–4801.
27 C. J. O'Sullivan and G. G. Guilbaut, *Biosens. Bioelectron.*, 1999, **14**, 663.
28 H. Liu and N. J. Hu, *J. Phys. Chem. B*, 2006, **110**, 14494.
29 Z. Feldötö, I. Varga and E. Blomberg, *Langmuir*, 2010, **26**, 17048.
30 H. Zhang, H. Lu and N. Hu, *J. Phys. Chem. B*, 2006, **110**, 2171.
31 F. Caruso, K. Niikura, D. N. Furlong and Y. Okahata, *Langmuir*, 1997, **13**, 3422.
32 D. A. Gorin, S. A. Portnov, O. A. Inozemtseva, Z. Luklinska, A. M. Yashchenok, A. M. Pavlov, A. G. Skirtach, H. Möhwald and G. B. Sukhorukov, *Phys. Chem. Chem. Phys.*, 2008, **10**, 6899.
33 M. Fang, P. S. Grant, M. J. McShane, G. B. Sukhorukov, V. O. Golub and Y. M. Lvov, *Langmuir*, 2002, **18**, 6338.
34 J. Fatisson, R. F. Domingos, K. J. Wilkinson and N. Tufenkji, *Langmuir*, 2009, **25**, 6062.
35 D. Xu, C. Hodges, Y. Ding, S. Biggs, A. Brooker and D. York, *Langmuir*, 2010, **26**, 18105.
36 V. M. Sukhov, O. V. Dement'eva, M. E. Kartseva, V. M. Rudoy and V. A. Ogarev, *Colloid J. (Transl. of Kolloidn. Zh.)*, 2004, **66**, 482.
37 J. J. Park, S. H. De Paoli Lacerda, S. K. Stanley, B. M. Vogel, S. Kim, J. F. Douglas, D. Raghavan and A. Karim, *Langmuir*, 2009, **25**, 443.
38 L. G. Paterno, M. A. G. Soler, F. J. Fonseca, J. P. Sinnecker, E. H. C. P. Sinnecker, E. C. D. Lima, M. A. Novak and P. C. Morais, *J. Phys. Chem. C*, 2009, **113**, 5087.
39 L. G. Paterno, M. A. G. Soler, F. J. Fonseca, J. P. Sinnecker, E. H. C. P. Sinnecker, E. C. D. Lima, S. N. Báo, M. A. Novak and P. C. Morais, *J. Nanosci. Nanotechnol.*, 2010, **10**, 2679.
40 S. Ayyappan, S. Mahadevan, P. Chandramohan, M. P. Srinivasan, J. Philip and R. J. Baldev, *J. Phys. Chem. C*, 2010, **114**, 6334.
41 S. Kückelhaus, S. C. Reis, M. F. Carneiro, A. C. Tedesco, D. M. Oliveira, E. C. D. Lima, P. C. Morais, R. B. Azevedo and G. R. Lacava, *J. Magn. Magn. Mater.*, 2004, **272–276**, 2402.
42 C. Cannas, A. Ardu, D. Peddis, C. Sangregorio, G. Piccaluga and A. Musinu, *J. Colloid Interface Sci.*, 2010, **343**, 415.
43 B. E. Kashevsky, V. E. Agabekov, S. B. Kashevsky, K. A. Kekalo, E. Y. Manina, I. V. Prokhorov and V. S. Ulashchik, *Particuology*, 2008, **6**, 322.
44 M. A. G. Soler, E. C. D. Lima, S. W. da Silva, T. F. O. Melo, A. C. M. Pimenta, J. P. Sinnecker, R. B. Azevedo, V. K. Garg, A. C. Oliveira, M. A. Novak and P. C. Morais, *Langmuir*, 2007, **23**, 9611.
45 J. Poplewell and L. Sakhnini, *J. Magn. Magn. Mater.*, 1995, **149**, 72.
46 International Center for Diffraction Data, PDF Card 22-1086, 2000.
47 G. Sauerbrey, *Z. Phys.*, 1959, **155**, 206.
48 R. F. M. Lobo, M. A. Pereira da Silva, M. Raposo, R. M. Faria and O. N. Oliveira Jr., *Nanotechnology*, 1999, **10**, 389.
49 H. Wang, C. Wang, C. Lei, Z. Wu, G. Shen and R. Yu, *Anal. Bioanal. Chem.*, 2003, **377**, 632.
50 D. S. Karpovich and G. J. Blanchard, *Langmuir*, 1994, **10**, 3315.
51 A. O. Ivanov and S. S. Kantorovich, *Colloid J.*, 2003, **65**, 189.
52 M. Semmler, E. K. Mann, J. Ricka and M. Borkovec, *Langmuir*, 1998, **14**, 5217.
53 M. Raposo, L. H. C. Mattoso and O. N. Oliveira Jr., *Thin Solid Films*, 1998, **327–329**, 739.
54 A. Marletta, R. A. Silva, P. A. Ribeiro, M. Raposo and D. Gonçalves, *Langmuir*, 2009, **25**, 2166.
55 A. O. T. Patrocinio, L. G. Paterno and N. Y. M. Ilha, *J. Phys. Chem. C*, 2010, **114**, 17954.
56 G. B. Alcantara, L. G. Paterno, F. J. Fonseca, P. C. Morais and M. A. G. Soler, *J. Magn. Magn. Mater.*, 2011, **323**, 1372.

